

Youssef Hammi

Center for Advanced Vehicular Systems,
Box 5405,
Mississippi State, MS 39762-5405
e-mail: yhammi@cavs.msstate.edu

Tonya W. Stone¹

Mem. ASME
Department of Mechanical Engineering,
Mississippi State University,
Box 9552,
Mississippi State, MS 39762-9552
e-mail: stone@me.msstate.edu

Bhasker Paliwal

Center for Advanced Vehicular Systems,
Box 5405,
Mississippi State, MS 39762-5405
e-mail: bhasker@cavs.msstate.edu

Mark F. Horstemeyer

Mem. ASME
Department of Mechanical Engineering,
Mississippi State University,
Box 9552,
Mississippi State, MS 39762-9552
e-mail: mforst@me.msstate.edu

Paul G. Allison

Mem. ASME
Department of Mechanical Engineering,
University of Alabama,
Box 870276,
Tuscaloosa, AL 35487-0276
e-mail: pallison@eng.ua.edu

Smooth Yield Surface Constitutive Modeling for Granular Materials

In this paper, the authors present an internal state variable (ISV) cap plasticity model to provide a physical representation of inelastic mechanical behaviors of granular materials under pressure and shear conditions. The formulation is dependent on several factors: nonlinear elasticity, yield limit, stress invariants, plastic flow, and ISV hardening laws to represent various mechanical states. Constitutive equations are established based on a modified Drucker–Prager cap plasticity model to describe the mechanical densification process. To avoid potential numerical difficulties, a transition yield surface function is introduced to smooth the intersection between the failure and cap surfaces for different shapes and octahedral profiles of the shear failure yield surface. The ISV model for the test case of a linear-shaped shear failure surface with Mises octahedral profile is implemented into a finite element code. Numerical simulations using a steel metal powder are presented to demonstrate the capabilities of the ISV cap plasticity model to represent densification of a steel powder during compaction. The formulation is general enough to also apply to other powder metals and geomaterials. [DOI: 10.1115/1.4034987]

1 Introduction

A constitutive model that captures the mechanical behavior of granular and frictional materials (soils, sands, concrete, rocks, ice, metal powder, etc.) can have different levels of complexity. A physically based, microstructure sensitive constitutive model is not only probably the most complex but also probably the most accurate for use in predictions. In particular, capturing the process–structure–property sequence requires that the physically based cause–effect interactions be included within the constitutive equations. During the densification process of granular materials, when an increasing pressure is applied, an initially loose granular material becomes increasingly cohesive, and its overall behavior tends to be similar to that of porous and dense materials. Piccolroaz et al. stated that modeling the mechanical process of compaction requires the description of the transition from a granular to a dense or even a fully dense (zero porosity) state [1]. In the transition between granular and fully dense states of a given material, the constitutive formulation faces the challenging problem of granular and dense materials having completely different mechanical behaviors, e.g., nonlinear elastic properties, cohesion, interparticle friction, pressure-sensitive yielding, plastic flow,

hardening laws, crack/fracture induced damage, differences in strength in triaxial extension versus compression, and the Bauschinger effect. Capturing these behaviors typically necessitates the use of fairly complicated and expensive nonlinear material models [2–11].

Since the early developments in the 1950s and 1960s by Drucker and Prager, plasticity theory has become an established framework for modeling the mechanical behavior of different metal and nonmetal materials [12]. Many critical state models for soils mechanics have been proposed to address the effects of stress state on geological types of materials, such as soils, sands, rock, and concrete [13–15]. These models were then adapted to partially saturated soils [16], pharmaceutical powders [17,18], cosmetic powders [19], ceramic and hard metal powders and most recently, for ductile metal powders [20,21]. For the case of macromechanical modeling of metal powder compaction, the cap model [22,23] and Cam-Clay model [24] are two of the most popular constitutive models. One of the pioneering extensions of metal plasticity theory to soil plasticity using the cap model was performed by Refs. [22,23] when they extended the von Mises yield criterion to capture the inelastic coupling between deviatoric and volumetric behaviors of many porous media. The basic cap model was first introduced when Ref. [25] proposed that the volumetric plasticity behavior of soils might be successfully modeled with a strain hardening compression cap surface that closes off the open end of the Drucker–Prager failure envelope. While preceding soil models and yield criteria, such as

¹Corresponding author.

Contributed by the Materials Division of ASME for publication in the JOURNAL OF ENGINEERING MATERIALS AND TECHNOLOGY. Manuscript received June 13, 2016; final manuscript received October 14, 2016; published online November 14, 2016. Assoc. Editor: Curt Bronkhorst.

Mohr–Coulomb, had captured frictional confinement strengthening behavior, this strain hardening model was one of the first that attempted to couple the deviatoric and volumetric compaction deformation behaviors of granular media. The role of the cap was to enhance the model in such a way as to include a representation of the phenomenon of soil compaction.

These models provide a powerful, yet adaptable way of representing many aspects of the dynamic stress–strain behavior of geological materials. The Drucker–Prager cap model is truly a unification of many classical plasticity models. For example, by using appropriate material parameters, this cap plasticity model can be instructed to behave precisely like a classical hardening or nonhardening von Mises model, in which case the yield surface becomes a cylinder centered about the (111) direction in the principal stress referential.

In general for porous metals, many compaction models [26–28] assume that tensile and compressive strengths are equal, partly because these models have been developed for the study of ductile fracture. Other models, such as the Cam-Clay model [24] or the Drucker–Prager model [22] for soil mechanics, assume a vanishing or a small cohesive strength between the particles. During the compaction of metal powders, the interparticle cohesive strength increases. Cohesion is a descriptive indication of interparticulate bonding behavior of powders. Fleck [29] proposed a material model with a variable degree of interparticle cohesion and introduced the cohesion factor, η , for which fully sticking contacts are obtained when $\eta = 1$, and zero cohesive strength is present at $\eta = 0$. In the last stage of compaction when the particles are mechanically bonded and the mechanism that controls the increasing density is mostly plastic deformation, the porous aggregate undergoes plastic hardening during plastic deformation arising from geometric effects (density change) or strain hardening [28]. During compaction, an increase in the material cohesion along the axis of the equivalent Mises stress is observed. In this work, the authors assume this increase in the material cohesion is representative of the plastic hardening mechanisms in addition to bonding due to diffusional effects.

The modeling of the mechanical process of compaction requires a description of the transition from a granular to a dense or even a fully dense state. Since granular materials are characterized by mechanical properties much different from those typical of dense solids, the constitutive model must describe a transition between two distinctly different states of a material. In this case, yielding becomes insensitive to pressure at high triaxialities, and the powder aggregate is characterized by a ductile behavior of near fully dense material. For example, Coube and Riedel [30] set a limit to the maximum possible equivalent Mises to avoid its value to reach unrealistically high stresses at the intersection of the cap and the failure line.

A successful model for the representation of the inelastic mechanical behavior should reflect the inter-particle cohesion, the frictional, and the compressible-densification yielding characteristics that have a major influence on the properties of the granular material. The granular model also needs the ability to describe the evolution of the porosity or density and the plasticity of the brittle/ductile particles with complex-shape geometries under multiaxial stress states. The density distribution is dependent on the combination of many factors, such as geometrical shape and mechanical properties of the aggregate. Therefore, the formulation of a physically based constitutive model needs to distinguish two different scales important during the deformation processes:

- The deformation of the aggregate idealized as a continuum—the classical macroscopic level.
- The deformation of the individual particles—the microscopic level.

To have an accurate description of the different scales, the following mechanical properties as defined by Trasorras et al. [31] should be part of the material model:

- Nonlinear elastic deformation of the granular aggregate.
- Nonlinear plastic deformation of the granular aggregate.
- Geometric hardening of the granular aggregate as a result of densification and a very large reduction in volume.
- Plastic deformation of the particles according to the behavior described by classical plasticity with isotropic hardening as the granular aggregate is compacted.
- Strain hardening of the metal powder particles.

To allow hardening of the failure shear envelope, the model should correlate the hardening of the overall aggregate with the plastic hardening of the particles and the density of the compacted material.

While numerical discretization techniques for plasticity models have been presented in the literature, performing implicit integration and analysis of constitutive equations using cap models remains a highly challenging task. One of the difficulties associated with most isotropic cap models is that the three independent surfaces comprising the yield surface do not intersect smoothly. It has been shown that the elastoplastic tangent operators at the corner points on such yield surfaces are singular, giving rise to potential numerical difficulties [32]. Many authors have developed cap model formulations by introducing yield surfaces smoothly connected, which eliminate the “corner coding” [2,3,33–35].

In this paper, a generalized ISV constitutive model for different types of granular materials is presented that includes the aforementioned essential qualities. The mathematical model is introduced as a combination of the modified Drucker–Prager/Cap model accounting for the lode-angle effect and a Mises type plasticity model within an ISV constitutive framework. A formulation for a smooth transitional surface between the shear failure envelope and cap surface is also introduced and can be applied to different nonlinear shear failure shapes and octahedral profiles. Furthermore, to avoid numerical singularities while dealing with the corner points in the octahedral plane on the corners, a parameter γ is introduced in the Lode function $\Gamma(\theta)$, which “smooths” the corners and makes them continuously differentiable. The failure envelope and the cap surface are defined as yield surfaces that are functions of the three stress invariants. As the formulation includes different mechanical properties of metal plasticity models, such as yield limit, rate sensitivity, isotropic hardening and kinematic hardening, it can also be used for porous and dense metallic materials. However, brittle/ductile fracture mechanisms of particles occurring at severe loading conditions, such as high shear loading, are not represented in this paper.

The approach herein differs from previous compaction models in that it combines the transition yield surface function with a modified lode angle definition to smooth corners of the octahedral profiles, and thereby a smooth transition equation is established for any shape and octahedral profile of the shear failure yield surface in order to avoid any potential numerical difficulties. The application to several different failure surface profiles is introduced and the compaction model is calibrated to a common copper steel powder. Densification of general granular materials is not as high as that in metallic powders. During compaction, metal powders deform and local plasticity at particle contacts allow for higher densification, which is accounted for in the ISV constitutive formulation presented in this work.

2 Plasticity for Granular Materials

To characterize the behavior of the granular aggregate, an ISV modified Drucker–Prager/Cap plasticity model based on the originally proposed work by DiMaggio and Sandler [36] for soil mechanics is used. This double surface plasticity model consists of an elastic region in stress space, bounded by a shear-failure surface, F_s , in the low pressure region and an elliptical yield cap surface, F_c , in the high pressure region. The mechanical behavior of granular media in compression can arise from adhesion and

frictional sliding at particle interfaces, fracture of particles, and plastic deformation of particles [37]. The yield/failure surfaces used with this model are written in terms of the three stress invariants: the hydrostatic stress,

$$p = -\frac{1}{3}\text{trace}(\boldsymbol{\sigma}) \quad (1)$$

the equivalent Mises stress,

$$q = \sqrt{\frac{3}{2}\mathbf{s} : \mathbf{s}} \quad (2)$$

and the third deviatoric stress invariant to reflect the behavioral features in triaxial extension and triaxial compression,

$$r = \left[\frac{9}{2}\mathbf{s} : \mathbf{s} : \mathbf{s} \right]^{\frac{1}{3}} \quad (3)$$

The deviatoric stress tensor \mathbf{s} is defined as

$$\mathbf{s} = \boldsymbol{\sigma} + p\mathbf{1} \quad (4)$$

where $\boldsymbol{\sigma}$ is the Cauchy stress tensor and $\mathbf{1}$ is the second-order unit tensor. Following standard conventions in soil mechanics, compression and compaction are assumed to be positive. The third invariant, r , influences only the Lode [38] angle, θ , also called the deviatoric polar angle, which determines the position (or triaxial state) of the stress point in the octahedral (deviatoric) plane and is defined by the following,

$$\theta = -\frac{1}{3} \sin^{-1} \left[\frac{r^3}{q^3} \right] \quad (5)$$

with $\theta \in [-30 \text{ deg}, 30 \text{ deg}]$. The Lode angle is a measurement of the intermediate principal stress, the value of which is -30 deg for triaxial compression and 30 deg for triaxial extension. The Lode angle is introduced in the yield surface expression through a Lode angle-dependent function, $\Gamma(\theta)$, which is discussed in Sec. 2.1.

2.1 Cap Model. In the original cap model proposed by DiMaggio and Sandler [36], the corner intersection or conditional branching between the two surfaces associated with the cap model, i.e., the failure envelope and cap yield surfaces, is a source of potential numerical instabilities. To eliminate this corner coding in the algorithm and have a better representation of experimental data, many authors [2–4,35] have utilized a nondimensional cap surface given by Pelessone [39] as

$$F_c(p, p_a) = 1 - H[p - p_a] \frac{[p - p_a]^2}{2[p_b - p_a]^2} = 0 \quad (6)$$

This cap surface is multiplied with the failure surface to form a smoothly varying and continuously differentiable capped-failure function. In Eq. (6), $H[\cdot]$ is the Heaviside function defined by

$$H[x] = \begin{cases} 1 & \text{if } x \geq 0 \\ 0 & \text{if } x < 0 \end{cases} \quad (7)$$

The cap hardening variable, p_a , is an evolution parameter that represents the volumetric plastic strain driven hardening/softening and controls the motion of the cap surface, and p_b defines the intersection of the cap surface with the pressure axis p (Fig. 1). The resulting capped-failure function is used to obtain the overall yield surface, which is given by Ref. [39] as

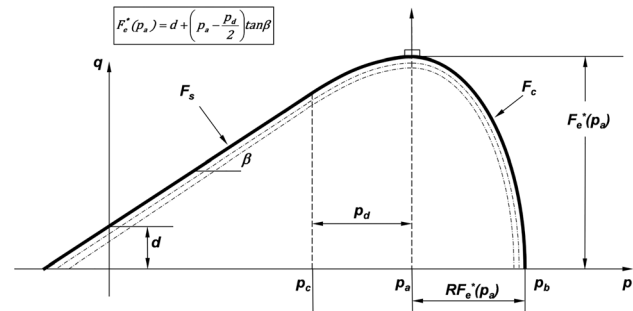


Fig. 1 The ISV cap model showing the yield surface in the meridional (q, p) plane

$$F(p, q, p_a) = q - F_s F_c(p, p_a) = 0 \quad (8)$$

where F_s is the shear failure yield surface.

In this work, the authors present a developed modified Drucker–Prager shear failure yield surface of the smooth cap model that accounts for the material’s density-dependent material cohesion and interparticle friction in addition to the Lode angle effect. The shear failure surface is defined as

$$F_s(p, q, \theta) = \Gamma(\theta)q - F_e^*(p) = 0 \quad (9)$$

with

$$F_e^*(p) = F_e(p) - f_i(p) \quad (10)$$

Here, the function $\Gamma(\theta)$ depends on the Lode angle θ to characterize the triaxial state of stress, $F_e(p)$ is a pressure-dependent function that defines the shape of the shear failure surface, and $f_i(p)$ is a transition function that smoothly connects the shear failure surface to the cap surface (the cap surface is described later in the section) in such a manner that the final capped yield surface is a continuously differentiable function. The function $F_e(p)$ is given by

$$F_e(p) = d + p \tan \beta \quad (11)$$

where the compaction material model parameters d and β represent cohesion and angle of friction, respectively, of the aggregate. Moreover, these parameters are allowed to vary with the density ρ of the aggregate, which evolves during the compaction/densification process as follows:

$$d = \begin{cases} 0 & \text{if } \rho < \rho_d \\ d_1 \exp[d_2(\rho - \rho_d)] - d_1 & \text{if } \rho \geq \rho_d \end{cases} \quad (12)$$

$$\tan \beta = \begin{cases} b_1 - b_2 \rho_d & \text{if } \rho < \rho_d \\ b_1 - b_2 \rho & \text{if } \rho \geq \rho_d \end{cases} \quad (13)$$

where ρ_d , d_1 , d_2 , b_1 , and b_2 are material parameters that can be determined from experiments on cylindrical samples [30]. Note that at low densities ($\rho < \rho_d$), material cohesion d is considered to be zero, and the interparticle friction β is considered to be constant.

2.2 Transitional Surface. The transitional function $f_i(p)$ is introduced in the failure yield surface, F_s , to define a smooth transitional yield function that connects the failure envelope and the cap surface. The pressure-dependent function $f_i(p)$ is defined by

$$f_i(p) = \frac{H[p - p_c]}{2(p_a - p_c)} [p - p_c]^2 \frac{\partial F_e(p)}{\partial p} \quad (14)$$

with

$$\frac{\partial F_c(p)}{\partial p} = \tan \beta \quad (15)$$

The function $H[p - p_c]$ is the Heaviside function

$$H[p - p_c] = \begin{cases} 1 & \text{if } p \geq p_c \\ 0 & \text{if } p < p_c \end{cases} \quad (16)$$

The variable p_c is defined by

$$p_c = p_a - p_d \quad (17)$$

where p_d is a material parameter initially set to a very small value. To have a smooth cap model, the failure envelope surface must be continuous with the cap yield surface, and therefore must verify the null-derivative condition at $p = p_a$ given by

$$\left. \frac{\partial F_c(p)}{\partial p} \right|_{p=p_a} = 0 \quad \forall p_a \quad (18)$$

It is noted that the procedure to obtain a continuously differentiable failure surface, which includes the shear failure surface F_s (Eq. (9)) along with the cap yield surface F_c (as defined in Eq. (21)), through the usage of transition functional, $f_t(p)$, is different from the procedure used in previous works (as shown in Eq. (8)). This approach also allows the use of a nonlinear shear failure surface continuously connected to the cap surface, examples of which are shown later in the section.

Sandler and Rubin [40] proposed a relationship called the isotropic cap hardening law to define the evolution of the cap's motion along the pressure axis with respect to the corresponding volumetric plastic strain

$$\bar{\epsilon}_{\text{vol}}^p = W(1 - \exp[-c_1(p_b - p_{b_0})^{c_2}]) \quad (19)$$

where W is the maximum plastic volumetric strain (at hydrostatic compression "lockup"), c_1 and c_2 are material shape factor parameters, and p_{b_0} is the initial value of p_b . Using the conservation of mass, the relative density (ratio of apparent density to theoretical "maximum" density), ρ , is derived from the plastic volumetric strain $\bar{\epsilon}_{\text{vol}}^p$ as follows:

$$\rho = \rho_0 \exp(-\bar{\epsilon}_{\text{vol}}^p) \quad (20)$$

where ρ_0 is the initial density or tap density.

2.3 Cap Yield Surface. The cap yield surface, F_c , has an elliptical shape in the meridional (q , p) plane (Fig. 1) and is written as

$$F_c = \sqrt{\Gamma(\theta)^2 q^2 - \frac{1}{R^2} [p - p_a]^2} - F_e^*(p_a) = 0 \quad (21)$$

where R is the cap eccentricity that controls the ellipsoidal shape of the cap. The cap hardening variable p_b that controls the motion of the cap surface is related to p_a as follows:

$$p_b = p_a + R F_e^*(p_a) \quad (22)$$

Finally, parameter R , which determines the ellipticity of the cap surface, is related to the density of the aggregate through the S-shaped sigmoid function described as follows:

$$R = R_0 + \frac{a}{1 + \exp\left[\frac{\rho_c - \rho}{b}\right]^c} \quad (23)$$

where R_0 is the initial cap eccentricity (the lower asymptote), a is the difference between the upper and lower asymptotes, ρ_c is the value of the density ρ at the point of inflection of the curve, and b and c exercise further control over the shape of the curve. Note that hardening caused by the density changes under pressure/shear loading not only expands the yield curve in the stress space but also causes the shape change as R is not a constant in our framework. This is in contrast with the previous works by Fossom and Brannon [3] in which R was assumed to be a constant.

Coube and Riedel [30] considered in their initial powder compaction model the cap eccentricity R , the material cohesion d , and the internal friction β to depend on the volumetric plastic strain. Coube and Riedel [30] also allowed in their second powder compaction model two material parameters, internal friction β and material cohesion d , to be internal state variables and functions of both volumetric and equivalent plastic strain rates. The evolution equations of these variables exhibit a more pronounced softening on the failure line, and the objective of this formulation is to describe the cracking as a process of strain localization.

2.4 Other Shear Failure Surfaces. The transitional surface $f_t(p)$ defined in Eq. (13) can also be used in conjunction with shear failure yield surfaces of different shapes, such as the hyperbolic form and a general exponent form (Figs. 2 and 3), to smoothly connect to the cap surface yield surface F_c (Eq. (20))

- hyperbolic form:

$$F_s = \sqrt{q^2 + (d'|_0 - p_t|_0 \tan \beta)^2} - F_c(p) + f_t(p) = 0 \quad (24)$$

$$F_e(p) = d' + p \tan \beta \quad (25)$$

$$\frac{\partial F_c(p)}{\partial p} = \tan \beta \Rightarrow f_t(p) = \frac{H[p - p_c]}{2(p_a - p_c)} [p - p_c]^2 \tan \beta \quad (26)$$

$$F_e^*(p_a) = \sqrt{\left[d' - \left(p_a - \frac{p_c}{2} \right) \tan \beta \right]^2 - (d'|_0 - p_t|_0 \tan \beta)^2} \quad (27)$$

- general exponent form:

$$F_s = a q^b - F_e(p) + f_t(p, p_a) = 0 \quad (28)$$

$$F_e(p) = p + p_t \quad (29)$$

$$\frac{\partial F_c(p)}{\partial p} = 1 \Rightarrow f_t(p) = \frac{H[p - p_c]}{2(p_a - p_c)} [p - p_c]^2 \quad (30)$$

$$F_e^*(p_a) = \sqrt{\frac{1}{a} \left(p_a + p_t - \frac{p_c}{2} \right)} \quad (31)$$

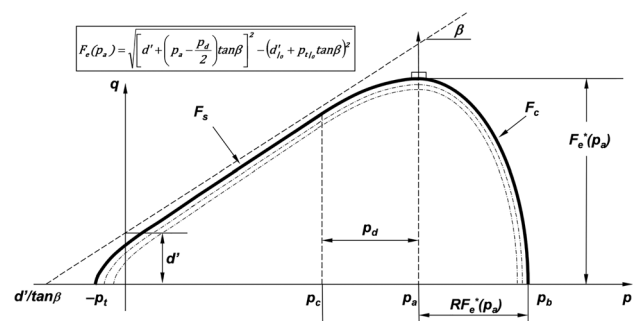


Fig. 2 Hyperbolic-shaped shear failure yield surface smoothly connected to a cap surface in the meridional (q , p) plane

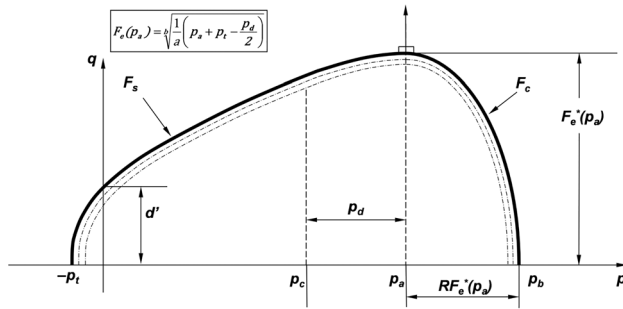


Fig. 3 Exponent-shaped shear failure yield surface smoothly connected to cap surface in the meridional (q, p) plane

A three-dimensional view of the linear, hyperbolic, and exponent-shaped shear failure surfaces smoothly connected to the cap surface is obtained by revolving the yield surface line in the meridional plane around the p -axis of pressure (Fig. 4).

2.5 Elastic Modulus. The cap model is used when the material being studied contains enough porosity (or highly compliant second phase inclusions) so that the inelastic volume reduction becomes possible through irreversible reduction of void space. Intuitively, one might expect the elastic moduli to stiffen as voids collapse. Many researchers have observed that the granular material model can be improved by updating the elastic and plastic properties (elastic moduli, cap eccentricity, material cohesion, internal friction, green strength) with the densification variable ρ (or the effective volumetric plastic strain $\bar{\epsilon}_{vol}^p$). The elastic Young's modulus, E , the shear modulus, G , and the bulk elastic modulus, K , can be deduced from the tests as a function of the density, ρ , and the Poisson's ratio, ν , can be derived from the shear and bulk moduli [41]. The elastic modulus as a function of the density is given by

$$E = (E_0 + E_1 \rho) \left[\exp\left(\frac{\rho}{\rho_0}\right) \right]^\gamma \quad (32)$$

where E_0 , E_1 , ρ_0 , and γ are material parameters and ρ is the density (g/cc).

Shear yield surface shapes and their octahedral profiles	Linear shape	Hyperbolic shape	Exponent shape
Mises profile			
Gudehus profile			
William-Warnke profile			
Mohr-Coulomb profile			

Fig. 4 Three-dimensional representation of the linear-, hyperbolic- and exponent-shaped shear yield surfaces smoothly connected to the cap surface with a Mises, Gudehus, William–Warnke, and Mohr–Coulomb octahedral profiles

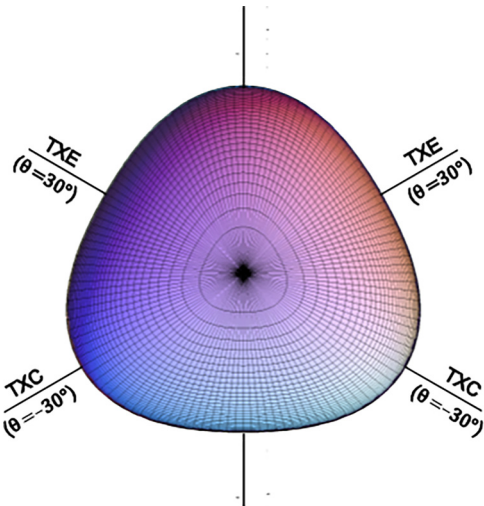


Fig. 5 Yield surface profile in the octahedral plane

2.6 Octahedral Profiles. In the material characterization of geomaterials, a triaxial extension (TXE) on cylindrical samples is obtained when the radial (or lateral) stress, σ_r , is increased while the axial stress, σ_a , is held constant, and the reverse is true for triaxial compression (TXC) tests. The triaxial laboratory tests on geomaterials exhibit the interesting phenomena that for a given mean stress, p , the triaxial extension tests will fail at a lower shear failure stress than the triaxial compression tests [42].

The triaxial stress state is usually characterized by the third invariant of the deviatoric stress tensor. Hence, in addition to the first and second stress invariants p and q , constitutive models are also function of the third stress invariant, r , through a Lode angle-dependent function $\Gamma(\theta)$ to reproduce more realistic failure in triaxial compression and extension (Fig. 5). Fossum and Brannon [3] have summarized in their Sandia Geomodel three different Lode angle-dependent functions:

- (1) Gudehus (an efficient smoothed profile, with restrictions on convexity):

$$\Gamma(\theta) = \frac{1}{2} \left[1 + \sin 3\theta + \frac{1}{\Psi} (1 - \sin 3\theta) \right] \quad (33)$$

- (2) Willam–Warnke (a relatively inefficient smooth profile with no convexity constraints):

$$\Gamma(\theta) = \frac{4(1 - \Psi^2) \cos^2 \alpha^* + (2\Psi - 1)^2}{2(1 - \Psi^2) \cos \alpha^* + (2\Psi - 1) \sqrt{4(1 - \Psi^2) \cos^2 \alpha^* + 5\Psi^2 - 4\Psi}} \quad (34)$$

where $\alpha^* = (\pi/6) + \theta$

- (3) Mohr–Coulomb (distorted hexagon polygon):

$$\Gamma(\theta) = \frac{2\sqrt{3}}{3 - \sin \theta} \left[\cos \theta - \frac{\sin \phi \sin \theta}{\sqrt{3}} \right] \quad (35)$$

where ϕ is determined from the user-supplied strength ratio $\sin \phi = 3((1 - \Psi)/(1 + \Psi))$

As shown on Fig. 6(a), the Gudehus and Willam–Warnke options both correspond to fully differentiable yield functions with no vertices. The Mohr–Coulomb option (which is available principally for comparisons with analytical solutions) is differentiable everywhere except at triaxial states where yield surface vertices require special numerical handling. To avoid these numerical singularities, we have introduced a parameter γ and replaced θ

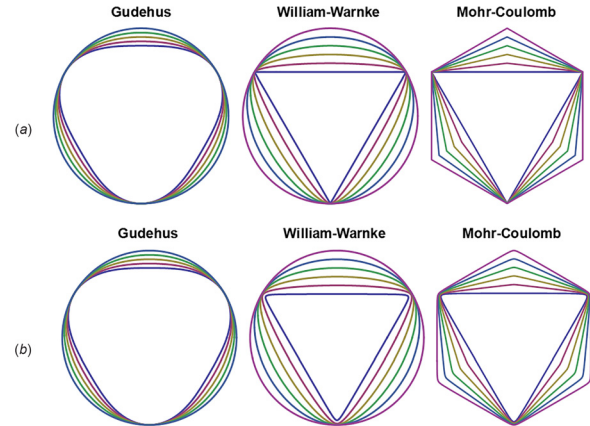


Fig. 6 Octahedral shear failure envelopes plotted at allowable values of strength ratio (a) with no smoothing and (b) with smoothing parameter, $\gamma = 0.995$

with $\bar{\theta}$ in the Lode function $\Gamma(\theta)$ [43] so that the deviatoric section can be shaped with a smoothing effect on the corners (see Fig. 6(b)). The replaced parameter $\bar{\theta}$ is given as

$$\bar{\theta} = \frac{1}{3} \sin^{-1} [\sin 3\gamma\theta] \quad (36)$$

The upper limit of the parameter γ is one (no effect) and the von Mises (circular) deviatoric section emerges when $\gamma = 0$. The three-dimensional graphical representation of the shear failure surface smoothly connected to the cap surface with a Mises octahedral profile can also be made with the different octahedral profiles that are Gudehus, Willam–Warnke, and Mohr–Coulomb (Fig. 4).

3 Material Model Calibration

The plasticity model with a linear shaped shear failure surface and a Mises octahedral profile as described above (see Fig. 1) was implemented into ABAQUS/EXPLICIT [44] via the user material subroutine VUMAT. A constant die wall friction value of 0.25 was used for the simulation. To calibrate the material parameters, different experimental tests are performed on cylindrical samples [45]. The material cohesion and interparticle friction were determined from compression and Brazilian tests at different densities. The cap eccentricity evolution, as function of density, was optimized using compaction simulations of cylindrical aggregates by comparing finite element values of hoop strains on the external surface of the die to strains measured during compaction experiments. The elastic Young’s modulus, E , and the bulk elastic modulus were deduced from resonant frequency tests as a function of density. All the experimental tests were combined to determine the evolution of the yield surface with respect to the relative density (% of theoretical “maximum” density). The calibrated material parameters are included in Table 1.

3.1 Cap Hardening—Compressibility Curves. The cap hardening describes the compressibility of the particulate material. It corresponds to the relationship between the plastic volumetric strain ε_{vol}^p and the stress tensor first invariant p_b , which is represented in the cap model as the intersection of the cap surface with the pressure p axis (see Fig. 1). The compressibility curve is ideally obtained from an isostatic compression of a loose powder specimen in an instrumented high pressure isostatic chamber. In the current study, two different FC-0205 copper steel powders were tested: Powder 1 and Powder 2 with 0.6% and 1.0%

Table 1 Powder compaction model parameters

Model	Variables	Value	Description
Density and elasticity	ρ_t	7.44	Theoretical density (g/cc or g cm ⁻³)
	ρ_0	3.1	Initial or tap density (g/cc or g cm ⁻³)
	E_0	30.0	Initial Young's modulus (MPa)
	E_1	60.0	Elastic parameter (MPa g ⁻¹ cm ³)
	ν	0.28	Poisson ratio
	γ	2.1	Exponent parameter
Failure envelope	d_1	0.08	Material cohesion parameter (MPa)
	d_2	0.5625	Material cohesion parameter
	b_1	6.3	Interparticle friction parameter
	b_2	5.26	Interparticle friction parameter
	ρ_d	0.4922	Relative density threshold
Cap surface	W	0.86	Cap hardening parameter
	c_1	0.168	Cap hardening parameter (1/MPa)
	c_2	0.413	Cap hardening parameter
	p_{d0}	0.00025	Cap hardening parameter (MPa)
	R_0	0.405	Initial cap eccentricity
	a	0.695	Difference between the upper and lower asymptotes
	b	2.0	Shape parameter of the eccentricity curve
	c	1.0	Shape parameter of the eccentricity curve
	ρ_c	0.97	Relative density at the point of inflection

Acrawax, respectively. The powder was enclosed in a flexible cylindrical container and tests were conducted at different pressures 70, 140, 210, 280, and 350 MPa using a cold isostatic pressing (CIP) equipment. After the powder aggregates were removed from the flexible container, each was cut into four pieces, and the density of each piece was measured using the immersion method [46]. The average densities of the aggregates are shown in Fig. 7 for each isostatic compaction test. An apparent density of 3.29 g/cc at zero pressure was considered in the calibration of material parameters, which explains the gap between the calibrated curve and data points at low pressure. The calibration process permits the determination of three important cap model parameters, W , c_1 , and c_2 , where W is a measure of the maximum achievable volumetric plastic strain.

3.2 Cohesion and Interparticle Friction—Brazilian and Compression Tests. To determine the material cohesion and interparticle friction parameters, d and β , compression and Brazilian disk tests were performed on cylindrical green samples of different densities ranging from 5.2 to 7.3 g/cc [30]. The Brazilian tests were performed according to ASTM D3967-95a [47]: *standard test method for splitting tensile strength of intact rock core specimens*. The compression tests were performed according to ASTM E9-89a [48] *Standard Test Methods of Compression*

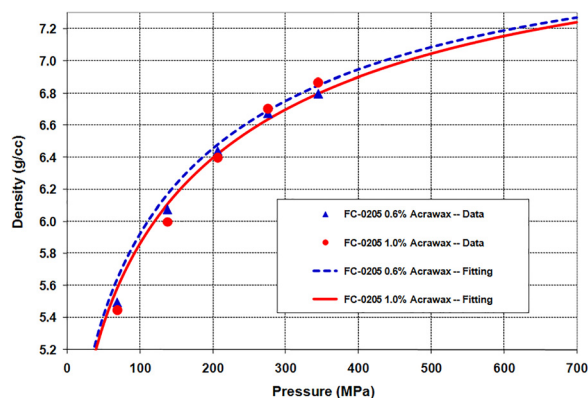


Fig. 7 Density–pressure compressibility curves associated with cap hardening for FC-0205 steel powders from isostatic compaction tests

Testing of Metallic Materials at Room Temperature. The fracture stresses, σ_c and σ_t , were measured, respectively, in the compression and Brazilian tests with different degrees of stress multiaxiality (Fig. 8).

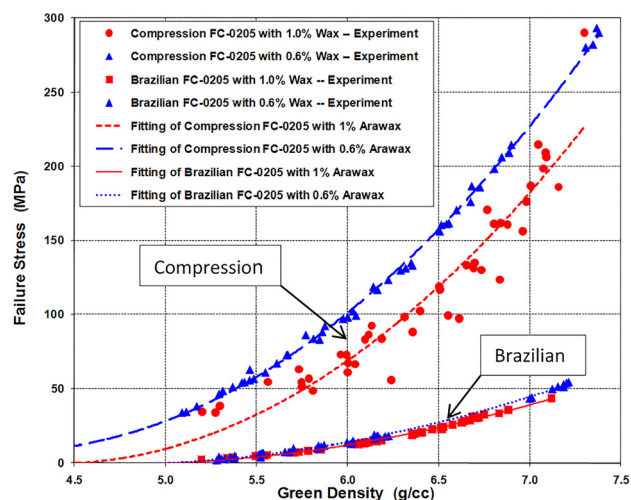


Fig. 8 Failure stress versus green density for FC-0205 steel cylindrical samples

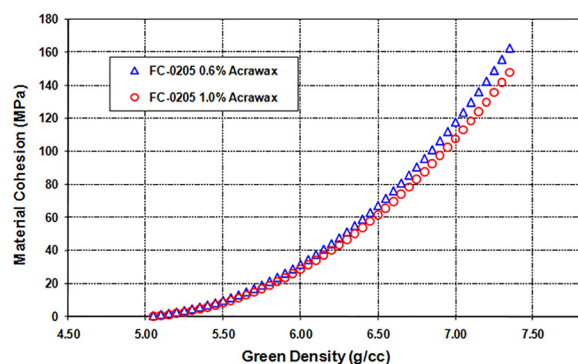


Fig. 9 Material cohesion (d) versus green density for FC-0205 steel cylindrical samples

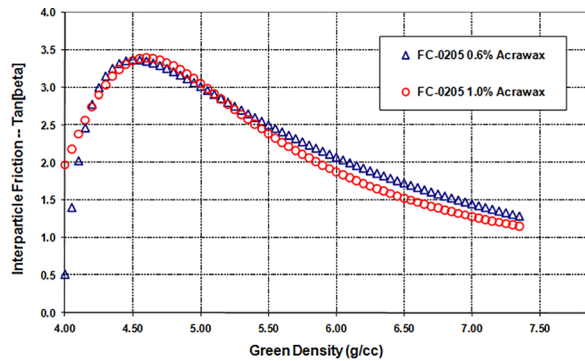


Fig. 10 Interparticle friction ($\tan \beta$) versus green density for FC-0205 steel cylindrical samples

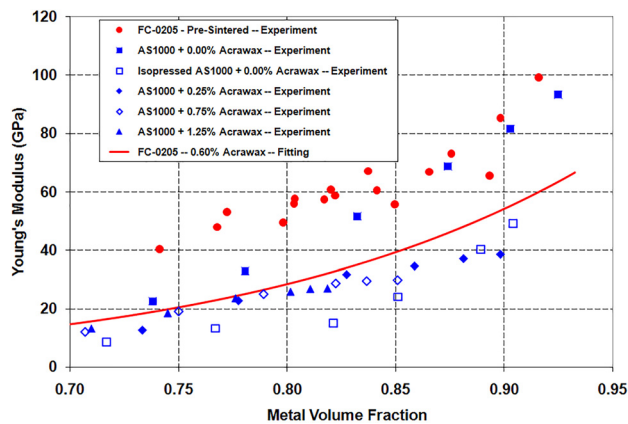


Fig. 11 Comparison of the elastic Young's modulus E as function of the porosity for the FC-0205 steel powder with the AS1000 metal powders (data from Ref. [51])

The equivalent Mises stresses, q_c and q_t , and the hydrostatic stresses, p_c and p_t , were calculated from the interpolation of the fracture stresses [30]:

$$p_c = \frac{\sigma_c}{3}, \quad q_c = \sigma_c \quad \text{and} \quad p_t = \frac{2\sigma_t}{3}, \quad q_t = \sqrt{13}\sigma_t \quad (37)$$

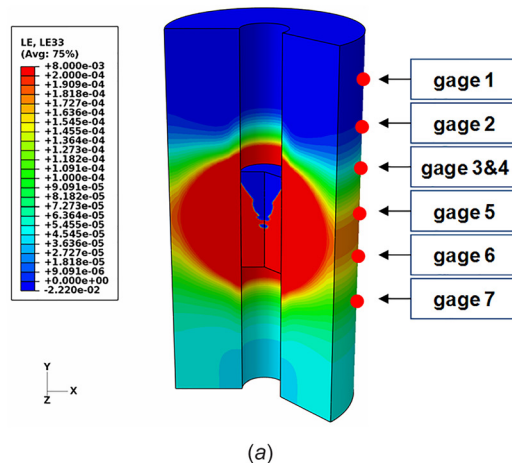


Fig. 12 (a) Hoop strain contours on the cylindrical die after simulated compaction of a FC-0205 copper steel powder and (b) strain gauges located on cylindrical die to measure hoop strain during compaction of FC-0205 powder

to determine the ordinate (d) and slope ($\tan \beta$) of the straight line failure envelope in the ISV cap model at different densities (Figs. 9 and 10).

3.3 Young's Modulus—Resonant Frequency Tests. Using the resonant frequency method [49], the Ultra RS laboratory in France determined the Young's modulus E of FC-0205 rectangular bars sized $3.2 \text{ cm} \times 1.7 \text{ cm} \times 0.64 \text{ cm}$ with green densities ranging from 5.6 to 7.2 g/cc . The Poisson's ratio is assumed constant and equal to 0.28 . The bulk modulus K and shear modulus G were derived from the Young's modulus E and Poisson's ratio ν functions of density [41]. Figure 11 shows variations of the Young's modulus with respect to the density (g/cc) for an iron-based powder.

3.4 Cap Eccentricity—Closed-Die Compaction Tests. The finite element method is an efficient numerical tool to improve the fundamental understanding of the mechanics of compaction but requires appropriate constitutive relations in terms of the evolution of suitable state variables for the full range of possible compaction mechanisms. It is a complementary technique to characterize a material parameter that is not directly measurable from testing [50]. To determine the cap eccentricity parameter in the ISV cap model, experimental and numerical simulations were performed on closed-die compaction of cylindrical powder aggregates. The cap eccentricity parameter was calibrated indirectly from the hoop strain. As shown in Fig. 12(b) strain gauges were attached to the external surface of a 5 cm diameter steel die to measure the hoop strain. Gauges 3 and 4 were located at the same distance from the bottom of the die but at different angles along the circumference. Compaction tests were performed on several FC-0205 powder cylinders of 1.7 cm diameter with different heights (2.54 cm , 3.8 cm , 5.0 cm , and 6.3 cm). The cap eccentricity parameter, R , which can be derived from the ratio of axial and radial stresses, was determined with an inverse method by comparing the numerical hoop strains to the measured hoop strains at different location on the die (Figs. 12(a) and 12(b)). The radial stress, exerted by the powder on the die wall, was calibrated by modifying the cap eccentricity parameter R in order to fit the strain gauge with the highest hoop strain as illustrated in Fig. 13. Differences in hoop strain (for densities up to 6.50 g/cc) between the experiment and finite element analysis are attributed to die wall friction, which was assumed to be constant in the finite element analysis model but varies in the experiment. After an iterative series of simulations, the cap eccentricity was calibrated for each powder as shown in Fig. 14.

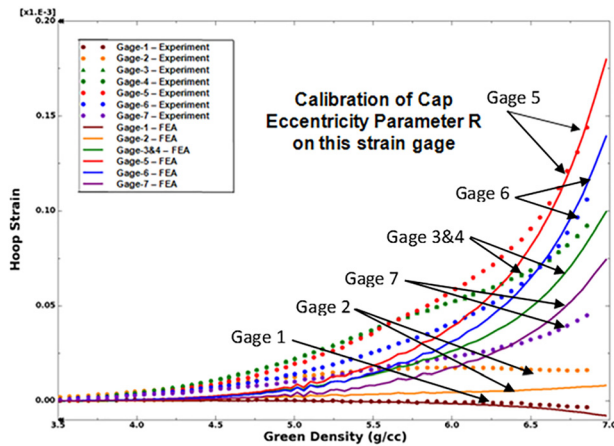


Fig. 13 Comparison of measured and finite element hoop strains for a 6.35 cm FC-0205 copper steel cylindrical sample

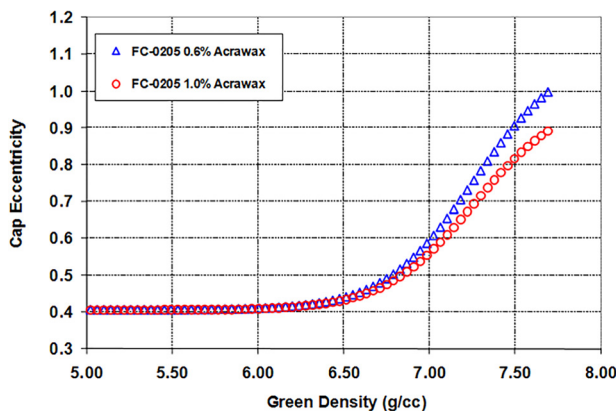


Fig. 14 Calibrated cap eccentricity versus green density for FC-0205 steel powders

3.5 Hydrostatic-Mises Stress— p - q -Plots. The previous Brazilian, compression, compressibility, and resonant frequency results were used to determine the failure line and cap surface for the FC0205 copper steel powder at different densities. Figure 15

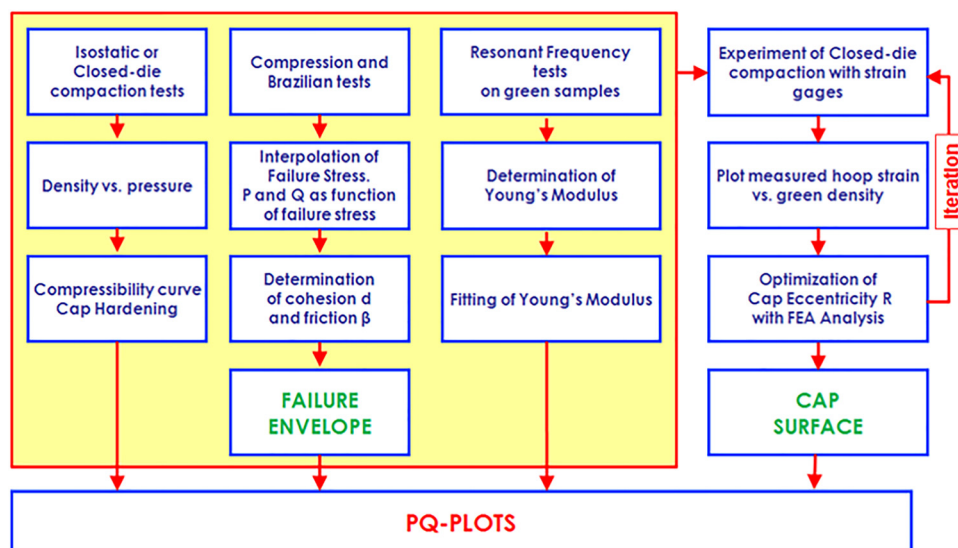


Fig. 15 Procedure to build p - q -plots from different experiments

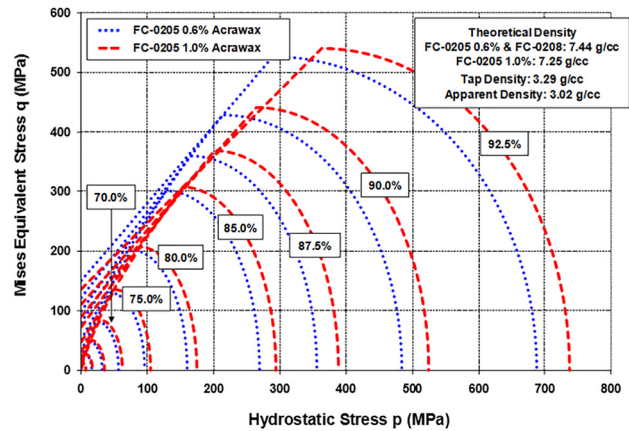


Fig. 16 Isodensity curves in the p - q meridional plane representing the evolution of the ISV cap model with respect to relative density (% theoretical) for FC-0205 steel powders

shows the procedure to build the p - q -plots (i.e., in the meridional plane) using data from the different tests. The compressibility curve, failure envelope, and Young's modulus curve were used as input data in finite element analyses that were performed to determine of the cap surface. Several trial-and-error iterations were needed in the case to calibrate experimental hoop strain versus density curves with numerical results to find the appropriate eccentricity of the cap surface at different densities. Figure 16 shows the equidensity lines in the p - q stress space, which correspond to the evolution of the failure envelope and cap surface of the ISV cap compaction model during densification. A smooth transition surface does not appear on the p - q -plots because of the small value of the parameter p_d (see Figs. 1–3).

4 Conclusions

A cap plasticity ISV model applied to the compaction of granular materials was introduced. To describe the different mechanical states of the granular media from loose to fully dense, the constitutive equations were developed using an ISV plasticity model with a Modified Drucker–Prager/Cap model at the continuum scale. A transitional function in the shear failure envelope was introduced to smoothly connect the failure yield surface to the elliptic cap surface and avoid future numerical instabilities. The

transitional function can be used with any shape of shear failure yield surface, such as the linear, hyperbolic, and exponent form, and also with different octahedral profiles. The model was finally calibrated for a common copper steel metal powder using experimental tests on cylindrical samples.

Acknowledgment

This paper is based upon work supported by the U.S. Department of Energy (DOE) National Energy Technology Laboratory under Award No. FC-26-02OR22910 with additional guidance from Russell A. Chernenkoff (Metaldyne), Shekhar G. Wakade (GM Powertrain), Eric McCarty (Materials Technologies Consulting LLC), Paulo Rosa (DaimlerChrysler), and Glen Weber (Ford Motor Company). We would like to acknowledge the Center for Advanced Vehicular Systems at Mississippi State University for supporting this work.

References

- Piccolroaz, A., Bigoni, D., and Gajo, A., 2006, "An Elastoplastic Framework for Granular Materials Becoming Cohesive Through Mechanical Densification—Part I: Small Strain Formulation," *Eur. J. Mech. A. Solids*, **25**(2), pp. 334–357.
- Schwer, L. E., and Murray, Y. D., 1994, "A Three-Invariant Smooth Cap Model With Mixed Hardening," *Int. J. Num. Anal. Methods Geomech.*, **18**(10), pp. 657–688.
- Fossum, A. F., and Brannon, R. M., 2004, "The Sandia Geomodel: Theory and User's Guide," Sandia National Laboratories, Albuquerque, NM, Report No. SAND2004-3226 UC-405.
- Foster, C. D., Regueiro, R. A., Fossum, A. F., and Borja, R. I., 2005, "Implicit Numerical Integration of a Three-Invariant, Isotropic/Kinematic Hardening Cap Plasticity Model for Geomaterials," *Comput. Methods Appl. Mech. Eng.*, **194**(50–51), pp. 5109–5138.
- La Ragione, L., Prantil, V. C., and Sharma, I. A., 2008, "Simplified Model for Inelastic Behavior of an Idealized Granular Material," *Int. J. Plast.*, **24**(1), pp. 168–189.
- Chandler, H. W., Sands, C. M., Song, J. H., Withers, P. J., and McDonald, S. A., 2008, "A Plasticity Model for Powder Compaction Processes Incorporating Particle Deformation and Rearrangement," *Int. J. Solids Struct.*, **45**(7–8), pp. 2056–2076.
- Yin, Z.-Y., and Chang, C. S., 2009, "Non-Uniqueness of Critical State Line in Compression and Extension Conditions," *Int. J. Numer. Anal. Methods Geomech.*, **33**(10), pp. 1315–1338.
- Chandler, H. W., and Sands, C. M., 2010, "Including Friction in the Mathematics of Classical Plasticity," *Int. J. Numer. Anal. Methods Geomech.*, **34**(1), pp. 53–72.
- Zhu, Q. Z., Shao, J. F., and Mainguy, M., 2010, "A Micromechanics-Based Elastoplastic Damage Model for Granular Materials at Low Confining Pressure," *Int. J. Plast.*, **26**(4), pp. 586–602.
- Kamrin, K., 2010, "Nonlinear Elasto-Plastic Model for Dense Granular Flow," *Int. J. Plast.*, **26**(2), pp. 167–188.
- Motamedi, M. H., and Foster, C. D., 2015, "An Improved Implicit Numerical Integration of a Non-Associated, Three-Invariant Cap Plasticity Model With Mixed Isotropic-Kinematic Hardening for Geomaterials," *Int. J. Numer. Anal. Methods Geomech.*, **39**(17), pp. 1853–1883.
- Sandler, I. S., 2005, "Review of the Development of Cap Models for Geomaterials," *Shock Vib.*, **12**(1), pp. 67–71.
- DorMohammadi, H., and Khoei, A. R., 2008, "A Three-Invariant Cap Model with Isotropic-Kinematic Hardening Rule and Associated Plasticity for Granular Materials," *Int. J. Solids Struct.*, **45**(2), pp. 631–656.
- Das, A., Tengattini, A., Nguyen, G. D., Viggiani, G., Hall, S. A., and Einav, I., 2014, "A Thermomechanical Constitutive Model for Cemented Granular Materials With Quantifiable Internal Variables—Part II: Validation and Localization Analysis," *J. Mech. Phys. Solids*, **70**, pp. 382–405.
- Tengattini, A., Das, A., Nguyen, G. D., Viggiani, G., Hall, S. A., and Einav, I., 2014, "A Thermomechanical Constitutive Model for Cemented Granular Materials With Quantifiable Internal Variables—Part I: Theory," *J. Mech. Phys. Solids*, **70**, pp. 281–296.
- Kohler, R., and Hofstetter, G., 2008, "A Cap Model for Partially Saturated Soils," *Int. J. Numer. Anal. Methods Geomech.*, **32**(8), pp. 981–1004.
- Han, L. H., Elliott, J. A., Bentham, A. C., Mills, A., Amidon, G. E., and Hancock, B. C., 2008, "A Modified Drucker–Prager Cap Model for Die Compaction Simulation of Pharmaceutical Powders," *Int. J. Solids Struct.*, **45**(10), pp. 3088–3106.
- Sinha, T., Bharadwaj, R., Curtis, J. S., Hancock, B. C., and Wassgren, C., 2010, "Finite Element Analysis of Pharmaceutical Tablet Compaction Using a Density Dependent Material Plasticity Model," *Powder Technol.*, **202**(1–3), pp. 46–54.
- Diarra, H., Mazel, V., Boillon, A., Rehault, L., Busignies, V., Bureau, S., and Tchoreloff, P., 2012, "Finite Element Method (FEM) Modeling of the Powder Compaction of Cosmetic Products: Comparison Between Simulated and Experimental Results," *Powder Technol.*, **224**, pp. 233–240.

- Bier, W., and Hartmann, S., 2006, "A Finite Strain Constitutive Model for Metal Powder Compaction Using a Unique and Convex Single Surface Yield Function," *Eur. J. Mech. A. Solids*, **25**(6), pp. 1009–1030.
- Heisserer, U., Hartmann, S., Düster, A., Bier, W., Yosibash, Z., and Rank, E., 2008, "P-FEM for Finite Deformation Powder Compaction," *Comput. Methods Appl. Mech. Eng.*, **197**(6–8), pp. 727–740.
- Drucker, D. C., and Prager, W., 1952, "Soil Mechanics and Plastic Analysis or Limit Design," *Q. Appl. Math.*, **10**(2), pp. 157–165.
- Drucker, D. C., 1953, "Limit Analysis of Two and Three Dimensional Soil Mechanics Problems," *J. Mech. Phys. Solids*, **1**(4), pp. 217–226.
- Schofield, A. N., and Wroth, C. P., 1968, *Critical State Soil Mechanics*, McGraw Hill, Maidenhead, UK.
- Drucker, D. C., Gibson, R. E., and Henkel, D. J., 1957, "Soil Mechanics and Work-Hardening Theories of Plasticity," *Trans. ASCE*, **122**, pp. 338–346.
- Gurson, A. L., 1977, "Continuum Theory of Ductile Rupture by Void Nucleation and Growth—Part I: Yield Criteria and Bow Rules for Porous Ductile Media," *ASME J. Eng. Mater. Technol.*, **99**(1), pp. 2–15.
- Shima, S., and Oyane, M., 1976, "Plasticity Theory for Porous Metals," *Inter. J. Mech. Sci.*, **18**(6), pp. 285–291.
- Fleck, N. A., Kuhn, L. T., and McMeeking, R. M., 1992, "Yielding of Metal Powder Bonded by Isolated Contacts," *J. Mech. Phys. Solids*, **40**(5), pp. 1139–1162.
- Fleck, N. A., 1995, "On the Cold Compaction of Powders," *J. Mech. Phys. Solids*, **43**(9), pp. 1409–1431.
- Coube, O., and Riedel, H., 2000, "Numerical Simulation of Metal Powder Die Compaction With Special Consideration of Cracking," *Powder Metall.*, **43**(2), pp. 123–131.
- Trasorras, J., Krauss, T. M., and Ferguson, B. L., 1989, "Modeling of Powder Compaction Using the Finite Element Method," *Adv. Powder Metall.*, **1**, pp. 85–104.
- Swan, C. C., and Seo, Y. K., 2000, "A Smooth, Three-Surface Elasto-Plastic Cap Model: Rate Formulation, Integration Algorithm and Tangent Operators," *University of Iowa*, Iowa City, IA.
- Desai, C. S., 1980, "A General Basis for Yield, Failure, and Potential Functions in Plasticity," *Int. J. Numer. Anal. Methods Geomech.*, **4**(4), pp. 361–375.
- Lade, P. V., and Kim, M. K., 1988, "Single Hardening Constitutive Model for Frictional Materials—Part I: Yield Criterion and Plastic Work Contours," *Comput. Geotech.*, **6**(1), pp. 13–29.
- Fossum, A. F., and Brannon, R. M., 2007, "On a Viscoplastic Model for Rocks With Mechanism-Dependent Characteristic Times," *Acta Geotech.*, **1**(2), pp. 89–106.
- DiMaggio, F. L., and Sandler, I. S., 1971 "Material Models for Granular," *J. Eng. Mech.*, **97**, pp. 935–950.
- Gurson, A. L., and McCabe, T., 1992, "Experimental Determination of Yield Functions for Compaction of Blended Metal Powders," *MPIF/APMI World Congress Powder Metall. Part. Mater.*, Vol. 1, pp. 21–26.
- Lode, W., 1926, "Versuche über den Einfluss der mittleren Hauptspannung auf das Fließen der Metalle Eisen Kupfer und Nickel. Z," *Agnew. Phys.*, **36**, pp. 913–939.
- Pelessone, D., 1989, "A Modified Formulation of the Cap Model," *Gulf Atomic, Technical Report No. GA-C 19579*.
- Sandler, I. S., and Rubin, D., 1979, "An Algorithm and a Modular Subroutine for the Cap Model," *Int. J. Numer. Anal. Methods Geomech.*, **3**(2), pp. 173–186.
- Pavier, E., and Doremus, P., 1999, "Triaxial Characterisation of Iron Powder Behavior," *Powder Metall.*, **42**(4), pp. 345–352.
- Launay, P., and Gachon, H., 1972, "Strain and Ultimate Strength of Concrete Under Triaxial Stress," *Spec. Publ.*, **34**, pp. 269–282.
- Bigoni, D., and Piccolroaz, A., 2003, "A New Yield Function for Geomaterials," *Constitutive Modelling and Analysis of Boundary Value Problems in Geotechnical Engineering*, Napoli, Italy, Apr. 22–24, C. Viggiani, ed., Hevelius, Benevento, Italy, pp. 266–281.
- ABAQUS, 2008, "ABAQUS: Theory Manual 6.8," Dassault Systèmes, Providence, RI.
- Majzoubi, G. H., and Jannesari, S., 2015 "Determination of the Constants of Cap Model for Compaction of Three Metal Powders," *Adv. Powder Technol.*, **26**(3), pp. 928–934.
- MPIF, 2010, "Method for Determination of Density of Compacted or Sintered Powder Metallurgy Products," *Metal Powder Industries Federation*, Princeton, NJ, Standard No. 42.
- ASTM, 2008, "Standard Test Method for Splitting Tensile Strength of Intact Rock Core Specimens," *ASTM International*, West Conshohocken, PA, Standard D3967-08.
- ASTM, 2009, "Standard Test Methods of Compression Testing of Metallic Materials at Room Temperature," *ASTM International*, West Conshohocken, PA, Standard E9-09.
- Birks, A. S., Green, R. E., and McIntire, P., 1991, *Ultrasonic Testing: Nondestructive Testing Handbook*, Vol. 7, American Society for Nondestructive Testing Inc., Columbus, OH, pp. 398–402.
- Sinka, I. C., Cunningham, J. C., and Zavaliangos, A., 2001, "Experimental Characterization and Numerical Simulation of Die Wall Friction in Pharmaceutical Powder Compaction," *PM2TEC 2001 International Conference on Powder Metallurgy & Particulate Materials*, New Orleans, LA, Vol. 1, pp. 46–60.
- Armstrong, S., Aesoph, M. D., and Gurson, A. L., 1995, "The Effects of Lubricant Content and Relative Powder Density on the Elastic, Yield and Failure Behavior of a Compacted Metal Powder," *Adv. Powder Metall. Part. Mater.*, **3**, pp. 31–44.